ACS Sustainable Chemistry & Engineering

pubs.acs.org/journal/ascecg

Research Article

Sodium Alginate as a Natural Substrate for Efficient and Sustainable Organic Solar Cells

Lorenzo Marchi, Franco Dinelli, Piera Maccagnani, Valentina Costa, Tatiana Chenet, Giada Belletti, Marco Natali, Massimo Cocchi, Monica Bertoldo,* and Mirko Seri*

Cite This: *ACS Sustainable Chem. Eng.* 2022, 10, 15608−15617

Read Online

ACCESS | Metrics & More | Article Recommendations | Supporting Information

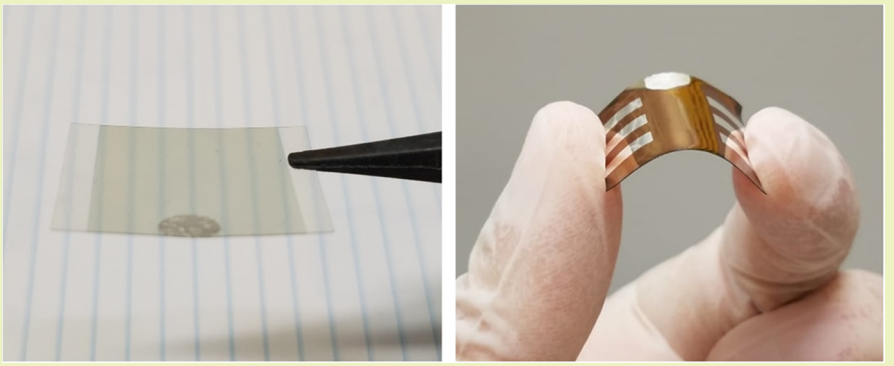

ABSTRACT: Organic electronics, in particular organic photovoltaics, have gained widespread attention due to their unique properties such as lightness, flexibility, and low cost. Thanks to some recent breakthroughs in organic solar cells (OSCs) that exhibit power conversion efficiencies (PCEs) approaching 20%, this technology is slowly making its way into the market as a complementary solution to conventional photovoltaic devices. OSCs are well suited for high-end smart applications, ranging from building integration and Internet of Things to consumer electronics. However, up to now, little attention has been devoted to the environmental impact and sustainability of components and processes. It is thus necessary to develop a new generation of eco-designed devices without losing the level of performance. In this work, we report the fabrication of efficient and stable solution-processed OSCs built on a free-standing sodium alginate (SA) substrate. SA is a natural biodegradable polymer derived from brown algae. It is low-cost, nontoxic, abundant, water-processable, and easy to manipulate for the realization of homogeneous and transparent foils. SA-based OSCs exhibit PCEs from 1.8 to 7.2% and can be disassembled through a safe and sustainable biocatalyzed process, allowing selective and almost entire recovery of precious metals, such as Au and Ag, as well as the separation of all of the main components. This allows us to minimize the production of e-waste, in accordance with the requirements of sustainability and the circular economy.

KEYWORDS: *organic solar cells, biomaterials, green electronics, sodium alginate, environmental sustainability*

INTRODUCTION

Bulk heterojunction (BHJ) organic solar cells (OSCs) offer great opportunities for the deployment of solar energy in new unexpected areas.[1−4] This is possible, thanks to their unique properties and remarkable merits such as low-cost manufacturing, reduced environmental impact (including the absence of toxic and rare elements), tunability of properties, and compatibility with ultrathin, lightweight, and flexible substrates. Research has made significant breakthroughs and progresses in terms of material design,[5,6] device architecture,[7] and processing conditions,[8,9] leading to state-of-the-art devices with power conversion efficiencies (PCEs) exceeding 19%.[10−12] The aforementioned specific and unique characteristics, combined with enhanced photovoltaic performance and proper operational lifetimes, highlight the great potential of OSCs for a widespread application range including building integration (indoor/outdoor), bioelectronics, self-powered (even wearable) devices, and Internet of Things (IoT).[13−18]

Despite the numerous challenges toward the commercial viability of this technology,[1,19] the production of customized lightweight and flexible OSCs is expected to rapidly increase in the near future, in particular considering their integration in smart products designed for relatively short life cycles or even

Received: September 20, 2022
Revised: November 2, 2022
Published: November 16, 2022

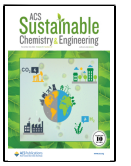

disposable applications. This could represent a real risk of generating a severe environmental impact deriving from a large amount of electronic wastes and nondegradable plastics, being flexible OSCs typically built on poly(ethylene terephthalate) (PET) or poly(ethylene naphthalate) (PEN) substrates.[18] This has fueled strong and multidisciplinary cooperation among researchers to develop new strategies for cost-effective preparation and implementation of natural and bio-derived (biodegradable) materials as alternative active and/or passive components for a new generation of eco-designed, flexible, and efficient OSCs.[20−24]

Among other possible material replacements, it is a matter of fact that the plastic substrate, due to its larger dimension and thickness compared to other layers, constitutes the bulk of the final device volume and weight. Therefore, its substitution with greener and biodegradable materials is an effective way to avoid the largest contribution to the total amount of generated waste. However, the choice of a biomaterial as an innovative substrate for OSCs is tricky. It should be ideally based on environmentally safe, i.e. biodegradable, abundant, and easily processable constituents, so as to not only avoid any environmental contamination risk but also reduce CO_2 emission associated to material origin and transformation. In addition, the resulting films also have to fulfill a series of specific requirements, such as (i) mechanical robustness and resistance, (ii) optical transparency, (iii) flexibility, (iv) surface homogeneity and smoothness, (v) compatibility with processing conditions, (vi) stability under operating/stress conditions, and (vii) low cost.[25]

Several biomaterials have been successfully tested in different electronic devices, both as passive and active components, as described in a number of comprehensive reviews.[26−29] Regarding substrates for OSCs, there are reports demonstrating the use of various biomaterials such as paper,[30−32] poly(vinyl alcohol),[33] cellophane,[34] and keratin.[35] To date, the best-performing solar cell was fabricated on a substrate of pretreated cellulose nanofibers (CNFs) with embedded silver nanowires (Ag-NWs). Using a highly efficient nonfullerene BHJ blend (PM6/Y6), Lin et al. prepared OSCs yielding a PCE up to 7.5% (vs 13.6% for the reference device on glass/ITO).[36] Remarkable results were also obtained using silk fibroin/Ag-NWs substrates. The resulting PTB7/PC_{71}BM-based OSCs led to a PCE of 6.6% (vs 7.9% for the reference device on glass/ITO).[37] PTB7/PC_{71}BM-based OSCs were also built on glossy paper, achieving a PCE of 6.4% (vs 7.5% for the reference device on glass/ITO).[38]

In this context, the encouraging results, described in one of our recent works on a vacuum-processed organic light-emitting diode (OLED) built on sodium alginate (SA),[39] have prompted us to further investigate the potential and versatility of this material, studying its compatibility even with solution processes. To this end, we report here the fabrication and characterization of BHJ OSCs built on transparent and conductive SA substrates. To date, SA has been used in OSCs only as an electron transport layer, as reported in some recent works.[40,41]

SA is a natural polysaccharide (chemical structure in Figure 2) derived from brown algae, with the great advantage of being relatively cheap, abundant, biocompatible, biodegradable, and water-soluble, allowing easy preparation of transparent and homogeneous ready-to-use free-standing films.[42] The resulting SA films have good resistance to common organic solvents,[43] good mechanical properties exhibiting plastic behavior and flexibility,[44] and exceptional oxygen barrier properties.[45,46] They can be opportunely functionalized with a thin pattern of Au to realize conductive substrates.[39,47,48] The resulting SA/Au foils have been used to build a set of inverted OSCs based on different BHJ blends: (i) P3HT/PC_{61}BM, (ii) PTB7/PC_{71}BM, and (iii) PTB7-Th/PC_{71}BM. On these devices, PCEs of 1.8, 5.4, and 7.2% have been obtained, respectively.

In addition, thanks to the composition of the substrate, the device can be disassembled through a safe and sustainable biocatalyzed process, allowing the selective recovery of the noble metals, as well as the separation of all of the main components, thus minimizing the production of electronic wastes, in accordance with the requirements of a circular economy.

EXPERIMENTAL SECTION

Materials. Acceptor materials PC_{61}BM ([6,6]-phenyl-C61-butyric acid methyl ester) and PC_{71}BM ([6,6]-phenyl-C71-butyric acid methyl ester) were purchased from Solenne BV, while donor polymers P3HT (poly(3-hexylthiophene-2,5-diyl), PTB7 (poly[[4,8-bis[(2-ethylhexyl)oxy]benzo[1,2-b:4,5-b′]dithiophene-2,6-diyl][3-fluoro-2-[(2-ethylhexyl)carbonyl]thieno[3,4-*b*]thiophenediyl]]), and PTB7-Th (poly[4,8-bis(5-(2-ethylhexyl)thiophen-2-yl)benzo[1,2-b;4,5-b′]dithiophene-2,6-diyl-alt-(4-(2-ethylhexyl)-3-fluoro thieno-[3,4-*b*]thiophene-)-2-carboxylate-2-6-diyl)]) were purchased from American Dye and Ossila. The commercial solution of ZnO (Helios ETL Slot Die H-SZ41029) was provided by Genes'Ink, while MoO_x was purchased from Sigma-Aldrich and used without further purification. Sodium alginate (SA) was purchased from Farmalabor Srl, (Canosa di Puglia (BT)). Analogously, all solvents and metals used for device fabrication were purchased from Sigma-Aldrich and used without further purification. Ag pellets (for electrode deposition) were purchased from Kurt J. Lesker.

Ultrapure water was produced with a Millipore Direct-Q 3UV (Merck kGaA, Burlington, MA, USA). EtOH 96% for analysis was purchased from Carlo Erba. Alginate lyase powder (≥10,000 units/g solid) was from Merck. HNO_3 69% (Suprapur) was purchased from Merck (Merck, Darmstadt, Germany); HCl 37% (Superpure) and H_2O_2 30% (ACS grade) were purchased from Carlo Erba (Carlo Erba Reagents, Milan, Italy). Multielement Standard solution 5 for ICP, Zn, Mo, and Ag, 10 mg L^{-1}, 10% HNO_3 (Trace CERT, Sigma-Aldrich, Steinheim, Germany) and Gold (Au) Pure Standard, 1000 μg/mL, 10% HCl (Perkin-Elmer, Waltham, MA) were used for the preparation of diluted standard solutions for calibration of ICP-MS.

Acetic acid (ReagentPlus >99%), ammonium hydroxide solution (NH_3, ACS Reagent 28−30%), chlorobenzene (ReagentPlus 99%), and all other solvents and metals used for device fabrication were purchased from Sigma-Aldrich and used without further purification.

ICP-MS Analysis. Metal concentration was determined by inductively coupled plasma mass spectrometry (ICP-MS); before analysis, samples were diluted with a solution containing 1% HNO_3 and 0.5% HCl, and all measurements were performed in triplicates. An Agilent 8800 Triple Quadrupole ICP-MS (Agilent Technologies, Santa Clara, CA) equipped with a MicroMist glass concentric nebulizer, a Peltier cooled double-pass Scott-type spray chamber, and Ni cones was used for the analyses. The instrument-optimized operating parameters were as follows: 1550 W RF power, 8.0 mm sampling depth, 15 L min^{-1} plasma gas, 1.03 L min^{-1} carrier gas, with the spray chamber temperature set at 2 °C, and the isotopes measured were ^{66}Zn, ^{95}Mo, ^{107}Ag, and ^{197}Au. The measurements were performed in He mode with a single-quad scan type. The He flow rate for the collision cell was 4.5 mL min^{-1}, and the integration time was 0.1 s for each mass value. The data acquisition was fixed at 3 replicates and 100 sweeps for replicates.

Preparation and Characterization of the SA Substrates. In accordance with reference 48, the SA films were obtained from solvent casting. First, a 4% SA solution was obtained by stirring together Milli-Q water and SA powder until reaching complete

https://doi.org/10.1021/acssuschemeng.2c05633
ACS Sustainable Chem. Eng. 2022, 10, 15608−15617

homogenization. Then, the solution was poured into a glass Petri dish and placed on a plane surface adjusted with the spirit level until dryness, typically for 3−4 days. The whole process was carried out inside a clean room under controlled environmental conditions: humidity ∼40% and temperature ∼23 °C. Homogeneous films with a thickness of 110 μm, as measured with a micrometer, were thus obtained. The Au deposition (∼8 nm) was carried out via sputtering in an MRC 8622 RF system applying a power of 20 W. Very low power was used to have fine control on the dimension of the Au nanoparticles, thickness, and penetration in the SA matrix. The amount of Au deposited was 4.6×10^{-4} g/g (9.2×10^{-6} g/cm^2) as obtained by ICP-MS analysis after digestion of the SA substrate (60 mg) with HNO_3/H_2O_2 3:1 (2 mL) at 130 °C for 4 h, and the separation of gold was performed by centrifugation and mineralization of the residue with freshly prepared aqua regia (1 mL of HNO_3/HCl 3:1) at 70 °C for 3 h.[49] Before analysis, the sample was diluted to 10 mL with Milli-Q water.

The optical properties (absorbance and transmittance spectra in the visible range) of films and complete devices were measured by a JASCO V-550 spectrophotometer. The thickness of nanometric layers was measured by a profilometer (KLA Tencor, P-6).

Device Fabrication and Characterization. The device architecture was glass/ITO/ZnO/BHJ layer/MoO_x/Ag or SA/Au/ZnO/BHJ layer/MoO_x/Ag. In agreement with reference 50, patterned ITO-coated glasses (Rs ∼10 Ω/square) were cleaned in sequential sonicating baths (for 15 min) in deionized water, acetone, and isopropanol. After the final sonication step, substrates were dried with a stream of Ar gas and then placed in an oxygen plasma chamber for 5 min. A thin layer of ZnO (∼40 nm) was spin-coated (in air) at 2000 rpm on top of the glass/ITO or SA/Au substrates. A preliminary test by spin-coating pure ethanol on top of the SA/Au substrate showed no change in its optical properties and planarity. Note that, the SA/Au substrates were adapted and temporarily attached (by biadhesive tape) to an additional support of glass to avoid deformations and/or movements during the spinning, thus favoring the deposition of different overlying layers. The active blend solutions were prepared as follows: (1) P3HT/PC_{61}BM (1:1 wt/wt) dissolved in chlorobenzene/*ortho*-dichlorobenzene (CB/ODCB, 1:1 v/v) with a total concentration of 50 mg/mL, (2) PTB7/PC_{71}BM (1:1.5 wt/wt) dissolved in CB with 3% (v/v) 1,8-diiodooctane (DIO) with a total concentration of 25 mg/mL, and (3) PTB7-Th/PC_{71}BM (1:2 wt/wt) dissolved in CB with 3% (v/v) 1,8-diiodooctane (DIO) with a total concentration of 21 mg/mL. All of the solutions were kept overnight at 65 °C under stirring. After dissolution, the active blends were spin-coated in air on top of glass/ITO/ZnO or SA/Au/ZnO substructures, using the following conditions: (1) P3HT/PC_{61}BM at 800 rpm for 120 s; (2) PTB7/PC_{71}BM at 1300 rpm for 120 s, and (3) PTB7-Th/PC_{71}BM at 2000 rpm for 120 s. Except for the P3HT/PC_{61}BM blend, thermally annealed at 80 °C for 10 min and 110 °C for 10 min when deposited on SA/Au and glass/ITO, respectively, no thermal treatments were carried out for PTB7- and PTB7-Th-based films. Then, the films were transferred inside the metal evaporator to complete the devices by depositing patterned MoO_x (10 nm) and Ag (average thickness 91 nm) layers. Ag thickness was measured from the amount deposited under comparable conditions on a glass slide (8×10^{-5} g) as determined by ICP-MS analysis after digestion with HNO_3 (1 mL) at 80 °C for 3 h and dilution with Milli-Q water to 10 mL.

Current−voltage (I−V) characteristics of all OSCs were recorded by a Keithley 236 source-measure unit under a simulated AM1.5G illumination of 100 mW/cm^2 (Abet Technologies Sun 2000 Solar Simulator) inside a glovebox. Note that, SA-based devices were peeled off from the glass substrate to obtain free-standing devices, thus avoiding optical interferences. The illuminated area (active area) of the photovoltaic cells was 6 mm^2. Indeed, during photovoltaic characterization (illumination), each cell was carefully masked with a calibrated mask with a spot of 6 mm^2.

The spectral response of the devices was recorded with a wavelength step size of 2 nm from 350 to 800 nm with a home-built system. Monochromatic light was generated by a xenon arc lamp from Lot-Oriel (300 Watt power) coupled with a monochromator (Spectra-Pro) by means of a parabolic mirror. The light beam was pulsed by means of an optical chopper (80 Hz frequency). The photocurrents generated in the devices and in the calibrated Si photodiode were recorded with a digital lock-in amplifier (Stanford Research Systems SR830).

The morphological characterization of the ZnO films, spin-coated on SA/Au substrates, was performed using an atomic force microscope (AFM) made of a commercial head (SMENA, NT-MDT), home-built electronics, and a digital lock-in amplifier (Zurich HF2LI). The setup was operated in intermittent contact mode (ICM). The cantilevers employed are commercially available from MikroMasch (HQ/NSC35).

Device Disassembling. The procedure consists of three steps, as depicted in Figure 5.

First Step. The top device layer consisting of six stripes of Ag and MoO_x was delaminated by immersion in 5 mL of ethanol in an ultrasound bath for 30 min. The other layers of the device were not affected by the treatment, and the device was collected, washed with 1 mL of fresh ethanol, and dried at room temperature. The delaminated layer portions were separated via centrifugation (Centrifuge DIAB D30249, 15,000 rpm for 5 min) and decantation. The dried solid was finally washed three times for 30 min with 1 mL of NH_3 0.5 M in an ultrasound bath (Ultrasound bath Elmasonic S40, 220−240V, 50/60Hz), centrifuged, and washed with water three times. The left solid was solubilized with 1 mL of HNO_3 at 80 °C for 3 h, diluted to 10.0 mL with ultrapure water, and analyzed by ICP-MS.[51]

Second Step. The second layer consisting of a mixture of a photoactive blend (PTB7-Th/PC_{71}BM) was washed off by gently shaking the device in 5 mL of chlorobenzene and then rinsing it with some fresh solvent. The solvent turned green/blue, while the device discolored, indicating the solubilization of the organic layer. The solvent was evaporated and the residuum was digested with 2 mL of HNO_3/H_2O_2 3:1 at 130 °C for 4 h, diluted to 10.0 mL with ultrapure water, and analyzed by ICP-MS.[52]

Third Step. The device (∼80 mg) was cut into small pieces, let to swell in 2 mL of water, then placed at 55 °C for 15 min, and mixed with a spatula. Alginate lyase was added (98 μL of a 5 U/mL enzyme solution). The mixture was incubated for another 15 min at 55 °C under vigorous stirring. Centrifugation at 15,000 rpm for 5 min allowed the supernatant to be separated and removed from the residuum. The residuum was washed three times with fresh water, then with 0.5 M acetic acid in an ultrasound bath for 30 min, and finally again with water. The solid residuum was dried, digested with 1 mL of freshly prepared aqua regia (HNO_3/HCl 1:3 by volume) for 3 h at 70 °C, diluted with Milli-Q water up to 10.0 mL, and analyzed by ICP-MS.[49] An AS220.R2 Balance (Radwag Wagi Elektroniczne) was used (max 220 g, min 10 mg).

RESULTS AND DISCUSSION

As already reported,[39,47] the deposition of a layer of Au with a small thickness (∼8 nm) on SA foils (∼110 μm) produces substrates with an optimal compromise between surface conductivity (17.0 Ω/sq) and optical and mechanical properties. Moreover, the resulting SA/Au substrate exhibits a uniform and smooth surface with a root-mean-square (RMS) roughness of ∼2.5 nm compared to ∼1.3 nm for the pristine SA film,[39] guaranteeing the quality of the overlying layers and the overall performances of the final device.

However, as opposed to vacuum-processed OLEDs, BHJ OSCs require substrates compatible with specific processing solvents. In particular, the choice of the first overlying layer and its processing conditions is of fundamental importance, being the physical and electrical connection between the SA/Au substrate and the upper part of the device. Using ZnO as a typical buffer layer for OSCs,[53] we have tested the wettability and the chemical/physical resistance of the hydrophilic SA/Au substrate spin-coating an alcoholic dispersion of ZnO nano-

https://doi.org/10.1021/acssuschemeng.2c05633
ACS Sustainable Chem. Eng. 2022, 10, 15608−15617

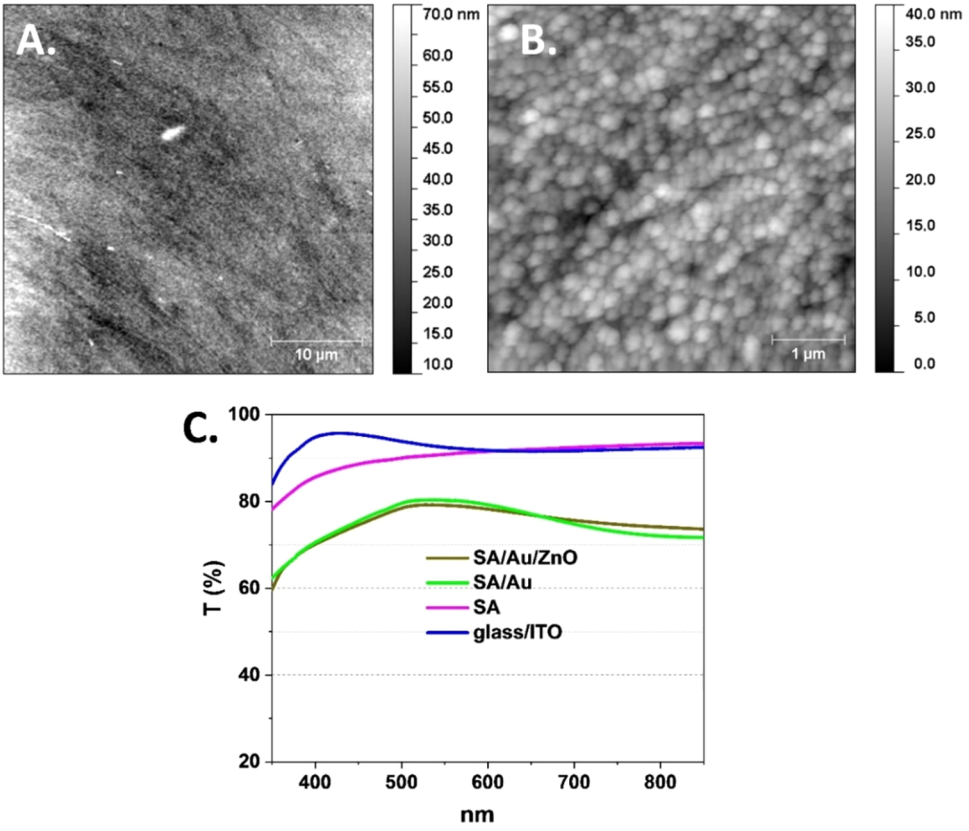

Figure 1. (A, B) AFM images (40 × 40 and 5 × 5 μm^2) of the ZnO layer spin-coated on a SA/Au substrate. (C) Optical transmission spectra of the various samples.

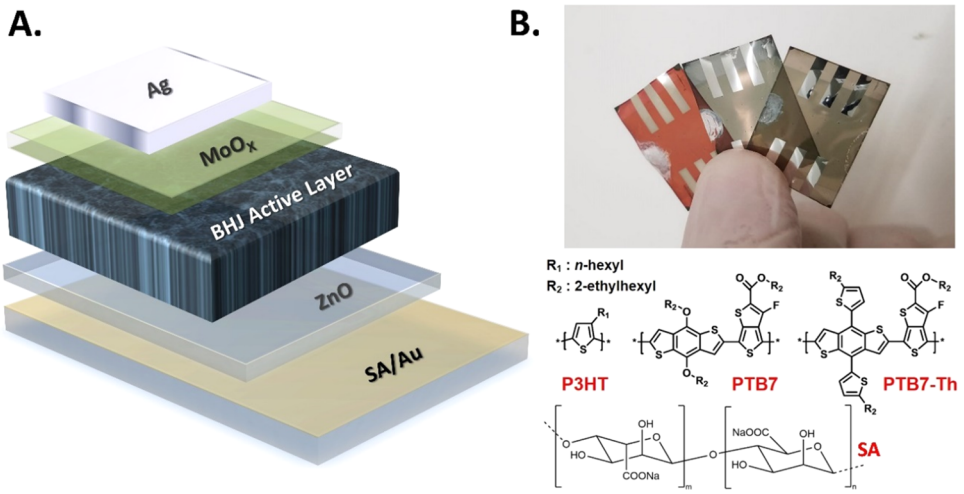

Figure 2. (A) Schematic structure of the SA-based inverted OSCs. (B) Top: complete SA-based OSCs; from the left: P3HT/$PC_{61}BM$ (1:1 wt/wt), PTB7/$PC_{71}BM$ (1:1.5 wt/wt), and PTB7-Th/$PC_{71}BM$ (1:2 wt/wt) based devices, and bottom: chemical structure of the donor materials employed and sodium alginate (SA).

particles (NPs) on that surface. As a result, we have obtained a continuous ZnO layer (~40 nm) without evidence of defects, aggregates, or uncovered areas. No macroscopic variation to the substrate properties, such as transparency and planarity, due to the solvent treatment occurred. The surface morphology of the ZnO layer has been investigated in detail with atomic force microscopy (AFM, Figure 1A,B). The ZnO layer is homogeneous, compact, and characterized by well-organized and finely nanostructured domains that uniformly cover the SA/Au surface.

The root-mean-square (RMS) roughness values of the ZnO surface are around ~9 and ~5 nm on areas of 40 × 40 and 5 × 5 μm^2, respectively. Compared to pristine SA (RMS: ~1 nm) and SA/Au (RMS: ~3 nm),[39] the ZnO layer exhibits slightly increased surface roughness. Nevertheless, the RMS roughness of the ZnO film is in perfect agreement with that of analogous films spin-coated on glass/ITO,[54] suggesting that the SA/Au substrate does not alter the nanoscale morphology and thus the intrinsic properties of the overlying ZnO layer. Regarding the optical transparency of the SA/Au films, Figure 1C

https://doi.org/10.1021/acssuschemeng.2c05633
ACS Sustainable Chem. Eng. 2022, 10, 15608−15617

Table 1. Device Responses, under Illumination, of Optimized P3HT/$PC_{61}BM$ (1:1 wt/wt), PTB7/$PC_{71}BM$ (1:1.5 wt/wt), and PTB7-Th/$PC_{71}BM$ (1:2 wt/wt) Inverted OSCs. The Reported Values are the Average of Five Different Solar Cells. The Values of the Best-Performing Devices are Reported in Square Brackets

BHJ active blend	substrate/cathode	J_{SC} (mA/cm^2)	V_{OC} (V)	FF (%)	PCE (%)
P3HT/$PC_{61}BM$	SA/Au	4.1 ± 0.3 [4.9][a]	0.58 ± 0.004 [0.58][a]	63 ± 2 [63][a]	1.5 ± 0.20 [1.8][a]
	glass/ITO	7.2 ± 0.3 [7.6][a]	0.58 ± 0.003 [0.59][a]	63 ± 3 [65][a]	2.7 ± 0.15 [2.9][a]
PTB7/$PC_{71}BM$	SA/Au	11.0 ± 0.4 [11.5][a]	0.71 ± 0.002 [0.71][a]	66 ± 1.5 [67][a]	5.2 ± 0.15 [5.4][a]
	glass/ITO	13.0 ± 0.3 [13.5][a]	0.75 ± 0.002 [0.75][a]	65 ± 0.5 [65][a]	6.4 ± 0.15 [6.6][a]
PTB7-Th/$PC_{71}BM$	SA/Au	13.2 ± 0.3 [13.9][a]	0.78 ± 0.002 [0.78][a]	65 ± 1 [66][a]	6.8 ± 0.15 [7.2][a]
	glass/ITO	16.4 ± 0.3 [16.4][a]	0.78 ± 0.003 [0.78][a]	64 ± 1.5 [66][a]	8.3 ± 0.10 [8.5][a]

[a]Maximum value, not considered for the average calculation.

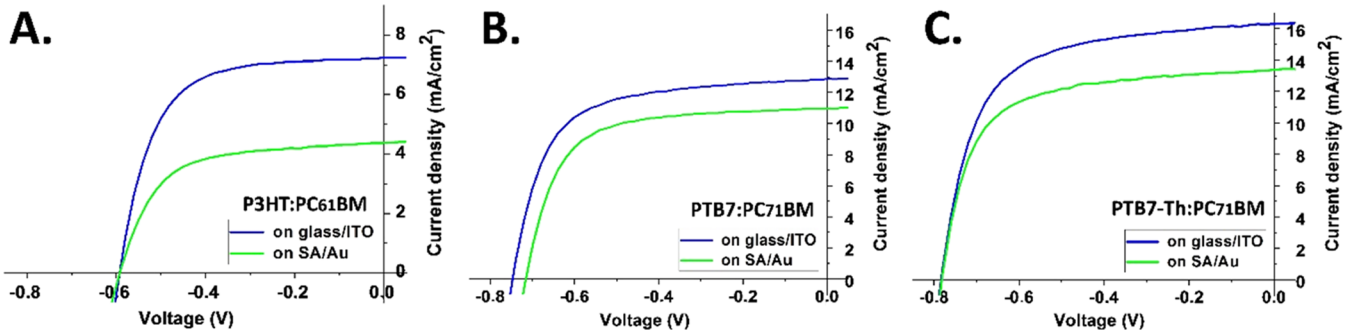

Figure 3. $J-V$ characteristics of (A) P3HT/$PC_{61}BM$ (1:1 wt/wt), (B) PTB7/$PC_{71}BM$ (1:1.5 wt/wt), and (C) PTB7-Th/$PC_{71}BM$ (1:2 wt/wt) inverted OSCs based on different substrates.

confirms that no change occurs after the ZnO deposition. The transmission spectrum of the SA/Au/ZnO substructure is nearly identical to that of SA/Au, with an average transmittance (AVT) of ∼75% for both systems. AVT is calculated from the arithmetic mean of the transmittance values recorded between 350 and 850 nm. For comparison, we also report in Figure 1C the transmission spectra of pristine SA and glass/ITO, which have AVT values of ∼90 and 92%, respectively.

This combination of optimal processability, coverage, and nanoscale morphology, including good optical transparency, makes this substructure a promising building block for a new generation of bio-based OSCs.

To test the potential and suitability of the SA/Au substrates in a complete device, a series of inverted solar cells, with the following structure SA/Au/ZnO/BHJ/MoO_x/Ag (Figure 2A), has been fabricated and characterized. Three different BHJ blends have been employed, P3HT/$PC_{61}BM$ (1:1 wt/wt), PTB7/$PC_{71}BM$ (1:1.5 wt/wt), and PTB7-Th/$PC_{71}BM$ (1:2 wt/wt), to investigate the behavior of SA-based solar cells using active layers with specific chemical, optical, morphological, and electrical characteristics (Figure 2B). The same sequences have been deposited on glass/ITO as reference devices and then tested. Additional details on the materials, processing conditions, and characterization are reported in the Experimental Section.

Table 1 summarizes the photovoltaic responses of all of the devices, including short-circuit current density (J_{SC}), open-circuit voltage (V_{OC}), fill factor (FF), and PCE, while Figure 3 exhibits the corresponding current density−voltage ($J-V$) plots. The $J-V$ curves of the best-performing devices are reported in Figure S1, corresponding to the data reported in parentheses in Table 1.

In general, the photovoltaic performance of our SA-based OSCs is slightly lower than that of analogous systems built on glass/ITO. Nevertheless, the PCE measured for the PTB7/$PC_{71}BM$ and PTB7-Th/$PC_{71}BM$ combinations passing from glass/ITO to SA/Au shows a reduction lower than 20%, a remarkable result if compared to similar studies on bio-based substrates reported in the literature.[22,55] This confirms the potential of the SA substrates, in particular their excellent compatibility with solution processes, allowing the deposition of multiple overlying layers.

The first set of OSCs has been devised as a preliminary test of the potential of SA as a substrate and thus prepared using the benchmark P3HT/$PC_{61}BM$ BHJ blend (Table 1). In detail, P3HT/$PC_{61}BM$ OSCs built on SA/Au (glass/ITO) substrates deliver a J_{SC} of 4.1 mA/cm^2 (7.2 mA/cm^2), a V_{OC} of 0.58 V (0.58 V), an FF of 63% (63%), and an average PCE of 1.5% (2.7%). As a result, a PCE decay of ∼40% has been observed passing from glass/ITO to SA/Au. The reduction in J_{SC} measured for the SA-based devices (4.1 vs 7.2 mA/cm^2) should be ascribed to optical losses due to the SA substrate and to slightly different conditions of the thermal annealing. The films have been annealed at 80 °C for 10 min in air, instead of 110 °C for 10 min using glass/ITO as a substrate, to prevent any possible deformation of the underlying natural support. No further optimization has been carried out for the P3HT/$PC_{61}BM$ OSCs built on SA/Au.

https://doi.org/10.1021/acssuschemeng.2c05633
ACS Sustainable Chem. Eng. 2022, 10, 15608−15617

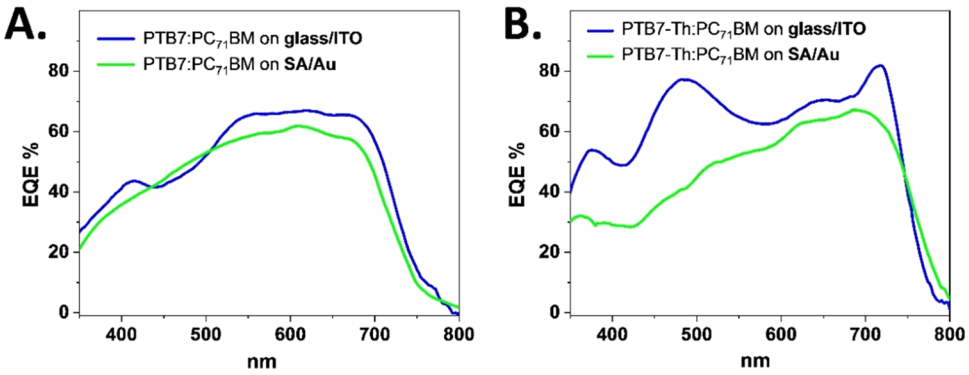

Figure 4. EQE spectra of (A) PTB7/$PC_{71}BM$ (1:1.5 wt/wt) and (B) PTB7-Th/$PC_{71}BM$ (1:2 wt/wt) based OSCs, built on glass/ITO and SA/Au substrates.

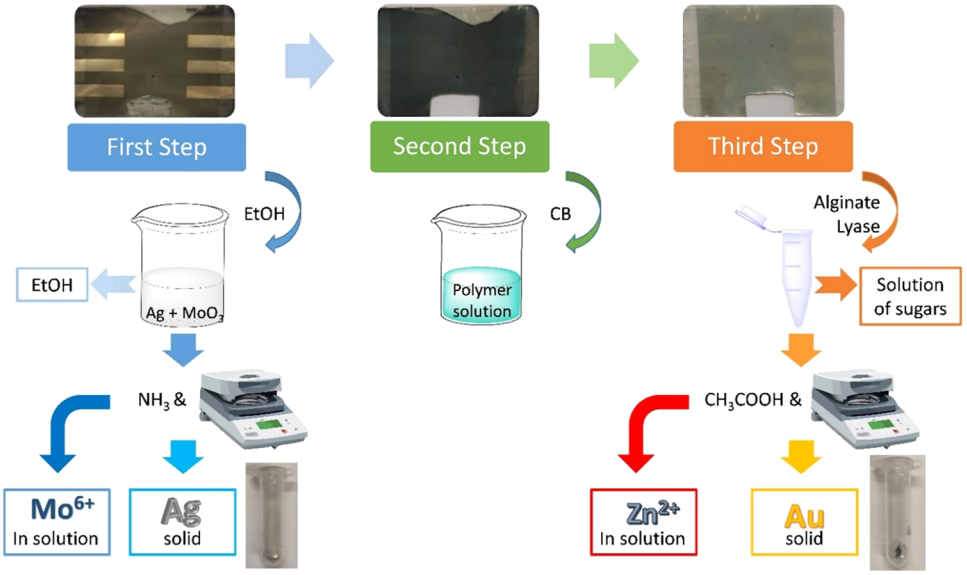

Figure 5. Scheme of the three-step disassembling procedure aiming at separating all of the components of the SA-based multilayer OSC.

The optimization of the efficiency has been obtained on the SA-based devices with more performant donor materials: PTB7 and PTB7-Th (Figure 2B). As a result, PTB7/$PC_{71}BM$ OSCs built on SA/Au (glass/ITO) substrates have delivered a J_{SC} of 11.0 mA/cm^2 (13.0 mA/cm^2), a V_{OC} of 0.71 V (0.75 V), an FF of 66% (65%), and an average PCE of 5.2% (6.4%). On the other hand, PTB7-Th/$PC_{71}BM$ devices on SA/Au (glass/ITO) substrates have given a J_{SC} of 13.2 mA/cm^2 (16.4 mA/cm^2), a V_{OC} of 0.78 V (0.78 V), an FF of 65% (64%), and an average PCE of 6.8% (8.3%). Maximum PCE values of 5.4 and 7.2% are obtained for SA-based devices containing PTB7 and PTB7-Th as donor materials, respectively (Table 1). Moreover, since both these BHJ blends are not subjected to thermal treatments, we observe a PCE decay of ∼18% passing from glass/ITO to SA/Au.

Looking at the photovoltaic parameters, it is evident that the main limiting factor of both SA-based devices, compared to the reference ones built on glass/ITO, is represented by J_{SC}. The V_{OC} and FF values, except for some small fluctuations, remain substantially unchanged, suggesting that SA/Au has almost no impact on some key related aspects, such as (i) energy level alignment within the device, (ii) quality of thin films and internal interfaces, without formation of defects and traps responsible for charge recombination/accumulation, and (iii) charge transport/extraction efficiency within the different layers and at the electrodes, without changes of the internal resistances (in series or parallel).[56]

As expected, the observed J_{SC} reduction can be mainly ascribed to the lower optical transparency of SA/Au compared to glass/ITO (AVT of ∼76 and 93%, respectively; Figure 1B), which hinders the light transmission toward the active blend, leading to devices with reduced photocurrents.

To exclude additional contributions to the J_{SC} reduction, due to morphology such as different self-organization of the BHJ blend as a function of the substrate, we have recorded and compared the UV−vis absorption spectra of the active blends deposited on both SA/Au and glass/ITO (Figure S2). Despite slightly different intensity values related to thickness variations, the different BHJ blends show a nearly identical spectrum, independent of the nature of the substrate. This confirms that the SA/Au foils, covered with a compact, homogeneous, and smooth ZnO buffer layer (Figure 1A,B), are solely responsible for the optical losses (J_{SC} reduction) without effects on the self-organization and all other related internal mechanisms of the overlying BHJ layers, in perfect agreement with the unchanged V_{OC} and FF values obtained for the analogous reference devices.

Figure 4 shows the external quantum efficiency (EQE) spectra of PTB7/$PC_{71}BM$ (1:1.5 wt/wt) and PTB7-Th/$PC_{71}BM$ (1:2 wt/wt) based OSCs, built on SA/Au and

https://doi.org/10.1021/acssuschemeng.2c05633
ACS Sustainable Chem. Eng. 2022, 10, 15608−15617

Table 2. Au, Ag, Zn, and Mo Amounts by the ICP-MS Analysis of the Fractions from the Disassembling Procedure Sketched in Figure 5 and the Corresponding Recovery Ratio, Calculated with Respect to the Metal Amount in the Device

sample	Au (μg)	recovery (%)	Ag (μg)	recovery (%)	Zn (μg)	recovery (%)	Mo (μg)	recovery (%)
Ag	0.2	0.7	69.2	80.5	0		0	
Mo^{6+} solution	0		4.6	5.4	0		0.92	32.7
EtOH	0		1.5	1.8	0		0.29	10.3
residuum CB	0.2	0.2	0.2	0.2	0		0	
Au	29.5	108.5	0.5	0.6	0		0	
SA solution	0.2	0.7	0.1	0.1	8.17	12.3	0.12	4.3
Zn^{2+} solution	<0.1	0.1	0		4.97	7.5	0	
TOTAL	29.95	**110.2**	76.12	**88.6**	13.14	**20%**	1.33	**47%**

glass/ITO substrates. The EQE profiles are consistent with the optical absorption spectra of the corresponding active blends (Figure S2). As expected, the lower intensity of the SA-based devices compared to those built on glass/ITO perfectly reflects the observed J_{SC} reduction (Table 1 and Figure 2), induced by the SA/Au substrate (Figure 1B). The convolution of the EQE spectra with the 1.5AM solar spectrum provides theoretical J_{SC} values (Table S1) in perfect agreement with those experimentally obtained from the $J-V$ measurements.

We have also preliminarily investigated the stability of the SA-based devices, monitoring the shelf life degradation of the best-performing PTB7 and PTB7-Th OSCs. To this end, SA-based solar cells have been kept in a glovebox for 2 months (not in dark) in the absence of oxygen and humidity and then remeasured to evaluate the evolution of their photovoltaic parameters. The absence of well-known degradation agents, such as water and oxygen, allows us to mainly ascribe eventual losses to morphological/chemical changes related to the SA substrate and/or to its adjacent interfaces. Interestingly, after 2 months of shelf storage, the solar cells built on SA, based on both PTB7/$PC_{71}BM$ and PTB7-Th/$PC_{71}BM$ blends, show a drop in PCE $\leq$ 8% (Table S2), indicating a good lifetime under these conditions. However, specific studies on the stability against light, heat, and other external stress factors, both on pristine SA substrates and complete devices, are currently underway and of crucial importance for further development.

The SA-based PTB7-Th/$PC_{71}BM$ OSC has been finally disassembled with an ad hoc three-step process. This methodology aims at separating all of the OSC components for the quantitative recovery of the noble metals, Ag and Au. Each step has been optimized to avoid or minimize the use of toxic substances. In particular, the last step is conducted with no use of synthetic chemicals exploiting an enzymatic-promoted bioprocess in water. In the whole procedure, when possible, chemicals already produced on an industrial scale from renewable resources, such as ethanol and acetic acid, have been selected in place of solvents derived from fossil oil and mineral acids. Besides, ammonia, rather than other mineral bases, can be produced directly from hydrogen and nitrogen,[57] both of which can be obtained from sustainable processes.[58]

The overall disassembling procedure is schematically represented in Figure 5. In the first step, the electrical contacts made of Ag on a thin layer of MoO_x can be peeled off by sonicating the full device in ethanol, a solvent that does not solubilize either SA[42,59] or the organic active blend.[60] A solid powder of Ag with MoO_x is recovered after centrifugation and it is purified by exploiting the selective solubility of MoO_x under basic conditions in NH_3.[61] Inductively coupled plasma mass spectrometry (ICP-MS) analysis of the residuum shows no detectable molybdenum and good recovery of Ag (Table 2). Based on the ICP analysis of all of the fractions obtained from the disassembling procedure (Figure 5), the largest loss of Ag occurs during the purification from MoO_x. In fact, 5% of Ag has been detected in the basic washing solution. However, this value can be underestimated, since some Ag may be lost by adsorbing onto the MoO_x precipitate that forms during the acid mineralization attack performed before the ICP analysis.

In the second step, the organic BHJ active layer is selectively washed off. For simplicity, we have used the solvent employed for the PTB7-Th/$PC_{71}BM$ deposition, namely, chlorobenzene (CB). Note that, alternative nontoxic halogen-free processing solvents can also be used for this purpose.[62−64] The procedure is very effective, since the amounts of Ag and Au detected in the residuum after solvent evaporation are almost negligible for both metals (Table 2).

The last step is represented by the separation of Au and ZnO from the SA film (3rd step in Figure 5). Theoretically, the easiest and most sustainable route is to solubilize the polysaccharide in neutral water for the recovery of the inorganic elements in a solid form. However, the high viscosity of the SA solution prevents the subsequent effective separation with centrifugation or filtration. In previous work, a similar step has been accomplished by promoting the desorption of Au from SA with a mixture of water and ethanol.[39] This mixture can be optimized to promote the swelling but not the solubilization of the SA film, thus avoiding the viscosity issue. Herein, we have developed an alternative method based on the reduction of the viscosity of the SA solution with enzymatic-promoted depolymerization of the polysaccharide. Alginate lyase, an enzyme able to cleave glycosidic bonds of the polysaccharide, has been used.[65] The cleaving condition can be initially optimized on model systems and then used in the third step of disassembling (Figure 5). To this aim, the remaining layers have been placed in water altogether in the presence of the enzyme. After incubation at the optimized conditions (55 °C for 15 min), the viscosity of the solution is below 0.06 Pa·s, and the inorganic components can be effectively separated with centrifugation. After washing the precipitate with an acetic acid solution to leach out ZnO,[66] ICP analysis can reveal the quantitative recovery of Au (Table 2). Furthermore, no zinc can be detected as an impurity. Zinc is, however, detected in both the water solution with depolymerized alginate and the leaching acid solution.

The apparent over-recovery of gold is due to the uncertainty on the initial amount present on the device due to broadening and thickness variation at the gold patterned edges.

https://doi.org/10.1021/acssuschemeng.2c05633
ACS Sustainable Chem. Eng. 2022, 10, 15608−15617

CONCLUSIONS

In this work, we have investigated the versatility and potential of SA/Au foils as natural and innovative substrates for applications in green electronics. Following our recent work on vacuum-processed organic light-emitting diodes,[39] we have used this innovative substrate to prepare flexible, efficient, and stable solution-processed organic solar cells (OSCs). These devices present power conversion efficiency (PCE) values up to 7.2%, compared to 8.5% obtained for analogous structures built on glass/ITO substrates. To our knowledge, the performances achieved are comparable to those obtained for the best-performing OSCs built on other bio-based substrates, such as silk fibroin/Ag-NWs (PCE: 6.6%),[37] glossy paper/Ag (PCE: 6.4%),[38] and pretreated cellulose nanofibers (CNFs) with embedded silver nanowires (Ag-NWs, PCE: 7.5%).[36] In addition, an environmentally safe disassembly method has been developed for the separation of all of the main components, obtaining selective and almost entire recovery of the noble metals (Ag and Au) employed. The overall procedure, starting from the fabrication to the disassembling of the BHJ OSCs, has been conceived with the aim of avoiding or at least minimizing the use of toxic and hazardous substances as well as the use of chemicals produced from fossil oil. The latter is important for reducing CO_2 emissions into the atmosphere. Therefore, our approach complies with the need for a more environmentally sustainable economy because not only of the possibility of producing clean energy using sunlight instead of burning fossil fuels but also of the low environmental impact of the device at all stages of its production and end-of-life management. Overall, the proposed method fits perfectly into the EU directives aiming at the transition to a more sustainable and circular economy.

ASSOCIATED CONTENT

Supporting Information

The Supporting Information is available free of charge at https://pubs.acs.org/doi/10.1021/acssuschemeng.2c05633.

J–*V* characteristics of the best-performing inverted OSCs; optical absorption spectra of different blends directly recorded on tested devices; theoretical J_{SC} values of optimized OSCs calculated from the convolution of the EQE spectra with the AM1.5 solar spectrum; and photovoltaic response before and after 60 days of shelf storage in a glovebox (PDF)

AUTHOR INFORMATION

Corresponding Authors

Monica Bertoldo − *National Research Council - Institute of Organic Synthesis and Photoreactivity (CNR-ISOF), 40129 Bologna, Italy; Department of Chemical, Pharmaceutical and Agricultural Sciences, University of Ferrara, 44121 Ferrara, Italy;* orcid.org/0000-0002-8221-2095; Email: brtmnc@unife.it

Mirko Seri − *National Research Council - Institute of Nanostructured Materials (CNR-ISMN), 40129 Bologna, Italy;* orcid.org/0000-0002-7868-5084; Email: mirko.seri@cnr.it

Authors

Lorenzo Marchi − *National Research Council - Institute of Organic Synthesis and Photoreactivity (CNR-ISOF), 40129 Bologna, Italy*

Franco Dinelli − *National Research Council - National Institute of Optics (CNR-INO), 56124 Pisa, Italy;* orcid.org/0000-0001-9467-4337

Piera Maccagnani − *National Research Council - Institute for Microelectronics and Microsystems, 40129 Bologna, Italy*

Valentina Costa − *Department of Environmental and Prevention Sciences, University of Ferrara, 44121 Ferrara, Italy*

Tatiana Chenet − *Department of Environmental and Prevention Sciences, University of Ferrara, 44121 Ferrara, Italy*

Giada Belletti − *National Research Council - Institute of Organic Synthesis and Photoreactivity (CNR-ISOF), 40129 Bologna, Italy; Department of Chemical, Pharmaceutical and Agricultural Sciences, University of Ferrara, 44121 Ferrara, Italy*

Marco Natali − *National Research Council - Institute of Nanostructured Materials (CNR-ISMN), 40129 Bologna, Italy*

Massimo Cocchi − *National Research Council - Institute of Organic Synthesis and Photoreactivity (CNR-ISOF), 40129 Bologna, Italy*

Complete contact information is available at: https://pubs.acs.org/10.1021/acssuschemeng.2c05633

Author Contributions

L.M. and G.B. worked on the experimental part and data discussion related to device disassembling. V.C. and T.C. worked on the analysis of metals through ICP-MS. F.D. and P.M. worked on the preparation, characterization, and optimization of SA and SA/Au substrates. M.N. and M.C. worked on the electrical characterization and data analysis of the fabricated photovoltaic devices. M.B. contributed to the writing of the manuscript and coordinated the data collection and discussion related to device disassembling. M.S. worked on device fabrication and optimization, coordinated the data collection and discussion related to photovoltaic devices, and wrote the manuscript. F.D. contributed significantly to the revision of the manuscript.

Notes

The authors declare no competing financial interest.

ACKNOWLEDGMENTS

The authors wish to thank Vincenzo Ragona (CNR-ISMN) for the valuable technical support. M.S. acknowledges funding from the Mission Innovation program MiSE under the Grant "Italian Energy Materials Acceleration Platform-IEMAP".

REFERENCES

(1) Seri, M.; Mercuri, F.; Ruani, G.; Feng, Y.; Li, M.; Xu, Z.-X.; Muccini, M. Toward Real Setting Applications of Organic and Perovskite Solar Cells: A Comparative Review. *Energy Technol.* **2021**, *9*, No. 2000901.

(2) Inganäs, O. Organic Photovoltaics over Three Decades. *Adv. Mater.* **2018**, *30*, No. 1800388.

(3) Cheng, H. W.; Zhao, Y.; Yang, Y. Toward High-Performance Semitransparent Organic Photovoltaics with Narrow-Bandgap Donors and Non-Fullerene Acceptors. *Adv. Energy Mater.* **2021**, *12*, No. 2102908.

(4) Chen, L. X. Organic Solar Cells: Recent Progress and Challenges. *ACS Energy Lett.* **2019**, *4*, 2537−2539.

(5) Gedefaw, D.; Tessarolo, M.; Bolognesi, M.; Prosa, M.; Kroon, R.; Zhuang, W.; Henriksson, P.; Bini, K.; Wang, E.; Muccini, M.; Seri, M.;

Andersson, M. R. Synthesis and Characterization of Benzodithiophene and Benzotriazole-Based Polymers for Photovoltaic Applications. *Beilstein J. Org. Chem.* **2016**, *12*, 1629−1637.
(6) Meredith, P.; Li, W.; Armin, A. Nonfullerene Acceptors: A Renaissance in Organic Photovoltaics? *Adv. Energy Mater.* **2020**, *10*, No. 2001788.
(7) Di Carlo Rasi, D.; Janssen, R. A. J. Advances in Solution-Processed Multijunction Organic Solar Cells. *Adv. Mater.* **2019**, *31*, No. 1806499.
(8) Prosa, M.; Tessarolo, M.; Bolognesi, M.; Cramer, T.; Chen, Z.; Facchetti, A.; Fraboni, B.; Seri, M.; Ruani, G.; Muccini, M. Efficient and Versatile Interconnection Layer by Solvent Treatment of PEDOT:PSS Interlayer for Air-Processed Organic Tandem Solar Cells. *Adv. Mater. Interfaces* **2016**, *3*, No. 1600770.
(9) Bolognesi, M.; Prosa, M.; Tessarolo, M.; Donati, G.; Toffanin, S.; Muccini, M.; Seri, M. Impact of Environmentally Friendly Processing on Polymer Solar Cells: Performance, Thermal Stability and Morphological Study by Imaging Techniques. *Sol. Energy Mater. Sol. Cells* **2016**, *155*, 436−445.
(10) Cui, Y.; Xu, Y.; Yao, H.; Bi, P.; Hong, L.; Zhang, J.; Zu, Y.; Zhang, T.; Qin, J.; Ren, J.; Chen, Z.; He, C.; Hao, X.; Wei, Z.; Hou, J. Single-Junction Organic Photovoltaic Cell with 19% Efficiency. *Adv. Mater.* **2021**, *33*, No. e2102420.
(11) Almora, O.; Baran, D.; Bazan, G. C.; Berger, C.; Cabrera, C. I.; Catchpole, K. R.; Erten-Ela, S.; Guo, F.; Hauch, J.; Ho-Baillie, A. W. Y.; Jacobsson, T. J.; Janssen, R. A. J.; Kirchartz, T.; Kopidakis, N.; Li, Y.; Loi, M. A.; Lunt, R. R.; Mathew, X.; McGehee, M. D.; Min, J.; Mitzi, D. B.; Nazeeruddin, M. K.; Nelson, J.; Nogueira, A. F.; Paetzold, U. W.; Park, N.; Rand, B. P.; Rau, U.; Snaith, H. J.; Unger, E.; Vaillant-Roca, L.; Yip, H.; Brabec, C. J. Device Performance of Emerging Photovoltaic Materials (Version 2). *Adv. Energy Mater.* **2021**, No. 2102526.
(12) Zhu, L.; Zhang, M.; Xu, J.; Li, C.; Yan, J.; Zhou, G.; Zhong, W.; Hao, T.; Song, J.; Xue, X.; Zhou, Z.; Zeng, R.; Zhu, H.; Chen, C.; MacKenzie, R. C. I.; Zou, Y.; Nelson, J.; Zhang, Y.; Sun, Y.; Liu, F. Single-Junction Organic Solar Cells with over 19% Efficiency Enabled by a Refined Double-Fibril Network Morphology. *Nat. Mater.* **2022**, *21*, 656−663.
(13) Ravishankar, E.; Booth, R. E.; Saravitz, C.; Sederoff, H.; Ade, H. W.; O'Connor, B. T. Achieving Net Zero Energy Greenhouses by Integrating Semitransparent Organic Solar Cells. *Joule* **2020**, *4*, 490−506.
(14) Jeong, E. G.; Jeon, Y.; Cho, S. H.; Choi, K. C. Textile-Based Washable Polymer Solar Cells for Optoelectronic Modules: Toward Self-Powered Smart Clothing. *Energy Environ. Sci.* **2019**, *12*, 1878−1889.
(15) Sun, B.; Li, Y. Ubiquitous Clean and Sustainable Energy-Driven Self-Rechargeable Batteries Realized by and Used in Organic Electronics. *J. Mater. Chem. C* **2022**, *10*, 388−412.
(16) Pecunia, V.; Occhipinti, L. G.; Hoye, R. L. Z. Emerging Indoor Photovoltaic Technologies for Sustainable Internet of Things. *Adv. Energy Mater.* **2021**, *11*, No. 2100698.
(17) Hashemi, S. A.; Ramakrishna, S.; Aberle, A. G. Recent Progress in Flexible−Wearable Solar Cells for Self-Powered Electronic Devices. *Energy Environ. Sci.* **2020**, *13*, 685−743.
(18) Liu, C.; Xiao, C.; Xie, C.; Li, W. Flexible Organic Solar Cells: Materials, Large-Area Fabrication Techniques and Potential Applications. *Nano Energy* **2021**, *89*, No. 106399.
(19) Moser, M.; Wadsworth, A.; Gasparini, N.; McCulloch, I. Challenges to the Success of Commercial Organic Photovoltaic Products. *Adv. Energy Mater.* **2021**, *11*, No. 2100056.
(20) Cavinato, L. M.; Fresta, E.; Ferrara, S.; Costa, R. D. Merging Biology and Photovoltaics: How Nature Helps Sun-Catching. *Adv. Energy Mater.* **2021**, *11*, No. 2100520.
(21) Kirschner, M. Why the Circular Economy Will Drive Green and Sustainable Chemistry in Electronics. *Adv. Sustainable Syst.* **2021**, *6*, No. 2100046.
(22) Bolognesi, M.; Prosa, M.; Seri, M. Biocompatible and Biodegradable Organic Electronic Materials. In *Sustainable Strategies in Organic Electronics*; Marrocchi, A. Elsevier, 2022; pp 297−338 DOI: 10.1016/B978-0-12-823147-0.00009-4.
(23) Kılıçarslan, B.; Bozyel, I.; Gökcen, D.; Bayram, C. Sustainable Macromolecular Materials in Flexible Electronics. *Macromol. Mater. Eng.* **2022**, *307*, No. 2100978.
(24) Li, X.; Ding, C.; Li, X.; Yang, H.; Liu, S.; Wang, X.; Zhang, L.; Sun, Q.; Liu, X.; Chen, J. Electronic Biopolymers: From Molecular Engineering to Functional Devices. *Chem. Eng. J.* **2020**, *397*, No. 125499.
(25) Li, X.; Li, P.; Wu, Z.; Luo, D.; Yu, H.-Y.; Lu, Z.-H. Review and Perspective of Materials for Flexible Solar Cells. *Mater. Rep.: Energy* **2021**, *1*, No. 100001.
(26) Li, W.; Liu, Q.; Zhang, Y.; Li, C.; He, Z.; Choy, W. C. H.; Low, P. J.; Sonar, P.; Kyaw, A. K. K. Biodegradable Materials and Green Processing for Green Electronics. *Adv. Mater.* **2020**, *32*, No. 2001591.
(27) Tan, M. J.; Owh, C.; Chee, P. L.; Kyaw, A. K. K.; Kai, D.; Loh, X. J. Biodegradable Electronics: Cornerstone for Sustainable Electronics and Transient Applications. *J. Mater. Chem. C* **2016**, *4*, 5531−5558.
(28) Huang, K. T.; Chueh, C. C.; Chen, W. C. Recent Advance in Renewable Materials and Green Processes for Optoelectronic Applications. *Mater. Today Sustainability* **2021**, *11*−*12*, No. 100057.
(29) Irimia-Vladu, M. "Green" Electronics: Biodegradable and Biocompatible Materials and Devices for Sustainable Future. *Chem. Soc. Rev.* **2014**, *43*, 588−610.
(30) Jayaraman, E.; Iyer, S. S. K. Organic Photovoltaic Modules Built on Paper Substrates. *Adv. Mater. Technol.* **2020**, *5*, No. 2000664.
(31) Nogi, M.; Karakawa, M.; Komoda, N.; Yagyu, H.; Nge, T. T. Transparent Conductive Nanofiber Paper for Foldable Solar Cells. *Sci. Rep.* **2015**, *5*, No. 17254.
(32) Hoeng, F.; Denneulin, A.; Bras, J. Use of Nanocellulose in Printed Electronics: A Review. *Nanoscale* **2016**, *8*, 13131−13154.
(33) Xi, H.; Chen, D.; Lv, L.; Zhong, P.; Lin, Z.; Chang, J.; Wang, H.; Wang, B.; Ma, X.; Zhang, C. High Performance Transient Organic Solar Cells on Biodegradable Polyvinyl Alcohol Composite Substrates. *RSC Adv.* **2017**, *7*, 52930−52937.
(34) Li, H.; Liu, X.; Wang, W.; Lu, Y.; Huang, J.; Li, J.; Xu, J.; Fan, P.; Fang, J.; Song, W. Realization of Foldable Polymer Solar Cells Using Ultrathin Cellophane Substrates and ZnO/Ag/ZnO Transparent Electrodes. *Solar RRL* **2018**, *2*, No. 1800123.
(35) Posati, T.; Aluigi, A.; Donnadio, A.; Sotgiu, G.; Mosconi, M.; Muccini, M.; Ruani, G.; Zamboni, R.; Seri, M. Keratin Film as Natural and Eco-Friendly Support for Organic Optoelectronic Devices. *Adv. Sustainable Syst.* **2019**, *3*, No. 1900080.
(36) Lin, P.-C.; Hsieh, C.-T.; Liu, X.; Chang, F.-C.; Chen, W.-C.; Yu, J.; Chueh, C.-C. Fabricating Efficient Flexible Organic Photovoltaics Using an Eco-Friendly Cellulose Nanofibers/Silver Nanowires Conductive Substrate. *Chem. Eng. J.* **2021**, *405*, No. 126996.
(37) Liu, Y.; Qi, N.; Song, T.; Jia, M.; Xia, Z.; Yuan, Z.; Yuan, W.; Zhang, K.-Q.; Sun, B. Highly Flexible and Lightweight Organic Solar Cells on Biocompatible Silk Fibroin. *ACS Appl. Mater. Interfaces* **2014**, *6*, 20670−20675.
(38) Rawat, M.; Jayaraman, E.; Balasubramanian, S.; Iyer, S. S. K. Organic Solar Cells on Paper Substrates. *Adv. Mater. Technol.* **2019**, *4*, No. 1900184.
(39) Cocchi, M.; Bertoldo, M.; Seri, M.; Maccagnani, P.; Summonte, C.; Buoso, S.; Belletti, G.; Dinelli, F.; Capelli, R. Fully Recyclable OLEDs Built on a Flexible Biopolymer Substrate. *ACS Sustainable Chem. Eng.* **2021**, *9*, 12733−12737.
(40) Zhang, X.; Shen, W.; Zhao, Y.; Wang, X.; Wang, Y.; Li, L.; Zhang, Y.; Long, Z.; Wang, J.; Belfiore, L. A.; Tang, J.; Inganäs, O. Non-Conjugated Natural Alginate as Electron-Transport Layer for High Performance Polymer Solar Cells after Modification. *J. Power Sources* **2021**, *510*, No. 230408.
(41) Zhang, X.; Shen, W.; Bu, F.; Wang, Y.; Yu, X.; Zhang, W.; Wang, J.; Belfiore, L. A.; Tang, J. Strong Enhanced Efficiency of Natural Alginate for Polymer Solar Cells through Modification of the ZnO Cathode Buffer Layer. *Appl. Opt.* **2020**, *59*, 9042.

(42) Pawar, S. N.; Edgar, K. J. Alginate Derivatization: A Review of Chemistry, Properties and Applications. *Biomaterials* **2012**, *33*, 3279−3305.
(43) Aburabie, J. H.; Puspasari, T.; Peinemann, K.-V. Alginate-Based Membranes: Paving the Way for Green Organic Solvent Nanofiltration. *J. Membr. Sci.* **2020**, *596*, No. 117615.
(44) Gheorghita Puscaselu, R.; Gutt, G.; Amariei, S. The Use of Edible Films Based on Sodium Alginate in Meat Product Packaging: An Eco-Friendly Alternative to Conventional Plastic Materials. *Coatings* **2020**, *10*, 166.
(45) Jost, V.; Kobsik, K.; Schmid, M.; Noller, K. Influence of Plasticiser on the Barrier, Mechanical and Grease Resistance Properties of Alginate Cast Films. *Carbohydr. Polym.* **2014**, *110*, 309−319.
(46) Hambleton, A.; Debeaufort, F.; Bonnotte, A.; Voilley, A. Influence of Alginate Emulsion-Based Films Structure on Its Barrier Properties and on the Protection of Microencapsulated Aroma Compound. *Food Hydrocolloids* **2009**, *23*, 2116−2124.
(47) Maccagnani, P.; Bertoldo, M.; Dinelli, F.; Murgia, M.; Summonte, C.; Ortolani, L.; Pizzochero, G.; Verucchi, R.; Collini, C.; Capelli, R. Flexible Conductors from Brown Algae for Green Electronics. *Adv. Sustainable Syst.* **2019**, *3*, No. 1900001.
(48) Barone, C.; Maccagnani, P.; Dinelli, F.; Bertoldo, M.; Capelli, R.; Cocchi, M.; Seri, M.; Pagano, S. Electrical Conduction and Noise Spectroscopy of Sodium-Alginate Gold-Covered Ultrathin Films for Flexible Green Electronics. *Sci. Rep.* **2022**, *12*, No. 9861.
(49) Mahmoud, N. N.; Alkilany, A. M.; Dietrich, D.; Karst, U.; Al-Bakri, A. G.; Khalil, E. A. Preferential Accumulation of Gold Nanorods into Human Skin Hair Follicles: Effect of Nanoparticle Surface Chemistry. *J. Colloid Interface Sci.* **2017**, *503*, 95−102.
(50) Albonetti, C.; El Qacemi, V.; Limage, S.; Versini, C.; Kauffmann, L. D.; Muccini, M.; Seri, M. Enhanced Thermal Stability of Inverted Polymer Solar Cells Based on Solution-Processed WOx as an Anode Interlayer. *Phys. Status Solidi A* **2021**, *2000748*, 1−11.
(51) Shameli, K.; Mansor Bin Ahmad, M.; Mohsen, Z.; Yunis, W. Z.; Ibrahim, N. A.; Rustaiyan, A. Synthesis of Silver Nanoparticles in Montmorillonite and Their Antibacterial Behavior. *Int. J. Nanomed.* **2011**, *6*, 581.
(52) Bakircioglu, D.; Kurtulus, Y. B.; Ucar, G. Determination of Some Traces Metal Levels in Cheese Samples Packaged in Plastic and Tin Containers by ICP-OES after Dry, Wet and Microwave Digestion. *Food Chem. Toxicol.* **2011**, *49*, 202−207.
(53) Liu, C.; Xiao, C.; Li, W. Zinc Oxide Nanoparticles as Electron Transporting Interlayer in Organic Solar Cells. *J. Mater. Chem. C* **2021**, *9*, 14093−14114.
(54) Prosa, M.; Tessarolo, M.; Bolognesi, M.; Margeat, O.; Gedefaw, D.; Gaceur, M.; Videlot-Ackermann, C.; Andersson, M. R.; Muccini, M.; Seri, M.; Ackermann, J. Enhanced Ultraviolet Stability of Air-Processed Polymer Solar Cells by Al Doping of the ZnO Interlayer. *ACS Appl. Mater. Interfaces* **2016**, *8*, 1635−1643.
(55) Li, W.; Liu, Q.; Zhang, Y.; Li, C.; He, Z.; Choy, W. C. H.; Low, P. J.; Sonar, P.; Kyaw, A. K. K. Biodegradable Materials and Green Processing for Green Electronics. *Adv. Mater.* **2020**, *32*, No. 2001591.
(56) Elumalai, N. K.; Uddin, A. Open Circuit Voltage of Organic Solar Cells: An in-Depth Review. *Energy Environ. Sci.* **2016**, *9*, 391−410.
(57) Ernst, F. A.; Reed, F. C.; Edwards, W. L. A Direct Synthetic Ammonia Plant. *Ind. Eng. Chem.* **1925**, *17*, 775−788.
(58) Sánchez, A.; Martín, M. Optimal Renewable Production of Ammonia from Water and Air. *J. Cleaner Prod.* **2018**, *178*, 325−342.
(59) Yeom, C. K.; Jegal, J. G.; Lee, K. H. Characterization of Relaxation Phenomena and Permeation Behaviors in Sodium Alginate Membrane during Pervaporation Separation of Ethanol-Water Mixture. *J. Appl. Polym. Sci.* **1996**, *62*, 1561−1576.
(60) Guo, S.; Cao, B.; Wang, W.; Moulin, J.-F.; Müller-Buschbaum, P. Effect of Alcohol Treatment on the Performance of PTB7:PC 71 BM Bulk Heterojunction Solar Cells. *ACS Appl. Mater. Interfaces* **2015**, *7*, 4641−4649.
(61) Zhao, Z.; Guo, M.; Zhang, M. Extraction of Molybdenum and Vanadium from the Spent Diesel Exhaust Catalyst by Ammonia Leaching Method. *J. Hazard. Mater.* **2015**, *286*, 402−409.
(62) Fu, Z.; Liu, X.; Niu, X.; Ren, M.; Xue, L.; Du, S.; Tong, J.; Li, J.; Bao, X.; Xia, Y. Enhancement Efficiency of Organic Photovoltaic Cells via Green Solvents and Nontoxic Halogen-Free Additives. *Adv. Sustainable Syst.* **2021**, *5*, No. 2100235.
(63) Campana, F.; Kim, C.; Marrocchi, A.; Vaccaro, L. Green Solvent-Processed Organic Electronic Devices. *J. Mater. Chem. C* **2020**, *8*, 15027−15047.
(64) Lee, S.; Jeong, D.; Kim, C.; Lee, C.; Kang, H.; Woo, H. Y.; Kim, B. J. Eco-Friendly Polymer Solar Cells: Advances in Green-Solvent Processing and Material Design. *ACS Nano* **2020**, *14*, 14493−14527.
(65) Zhu, B.; Yin, H. Alginate Lyase: Review of Major Sources and Classification, Properties, Structure-Function Analysis and Applications. *Bioengineered* **2015**, *6*, 125−131.
(66) EFSA Panel on Food Contact Materials Flavourings and Processing Aids (CEF), Electrical Conduction and Noise Spectroscopy*EFSA J.***2016***144*408 DOI: 10.2903/j.efsa.2016.4408.